INTERNATIONAL JOURNAL FOR NUMERICAL METHODS IN ENGINEERING
Int. J. Numer. Meth. Engng (2017)
Published online in Wiley Online Library (wileyonlinelibrary.com). DOI: 10.1002/nme.5499

Randomized dynamic mode decomposition for nonintrusive reduced order modelling

Diana Alina Bistrian[1] and Ionel Michael Navon[2]

[1]*Department of Electrical Engineering and Industrial Informatics, Politehnica University of Timisoara, Hunedoara, 331128, Romania*
[2]*Department of Scientific Computing, Florida State University, Tallahassee, 32306-4120, FL, USA*

SUMMARY

This paper focuses on a new framework for obtaining a nonintrusive (i.e., not requiring projecting of the governing equations onto the reduced basis modes) reduced order model for two-dimensional fluid problems. To overcome the shortcomings of intrusive model order reduction usually derived by combining the Proper Orthogonal Decomposition and the Galerkin projection methods, we developed a novel technique on the basis of randomized dynamic mode decomposition (DMD) as a fast and accurate option in model order reduction. Our approach utilizes an adaptive randomized DMD to obtain a reduced basis in the offline stage, and then the temporal values of the reduced order model are obtained in the online stage through an interpolation using radial basis functions. The rank of the reduced DMD model is given as the unique solution of a constrained optimization problem. The Saint-Venant (shallow water) equations in a channel on the rotating earth are employed to provide the numerical data. We emphasize the excellent behavior of the nonintrusive reduced order model by performing a qualitative analysis. In addition, we gain a significantly reduction of CPU time in computation of the reduced order models compared with the classical DMD method.

Received 12 October 2016; Revised 17 December 2016; Accepted 20 December 2016

KEY WORDS: randomized dynamic mode decomposition; nonintrusive reduced order modelling; randomized SVD

1. INTRODUCTION, FOCUS, AND MOTIVATION

The current line of this survey is motivated by the efficiency of reduced order modelling (ROM) in different problems arising in hydrodynamics, where data are collected in the aftermath of an experiment or are provided by measurement tools. We refer to this data as nonintrusive data. In the context of application of mathematical and numerical techniques for modelling the nonintrusive massive data, the intent of this paper is to undertake an efficient technique of model order reduction of shallow water systems. The challenge of this task is to build a linear dynamical system that models the evolution of the strongly nonlinear flow and to define a new mathematical and numerical methodology for studying dominant and coherent structures in the flow.

Among several model order reduction techniques, Proper Orthogonal Decomposition (POD) and Koopman Mode Decomposition represent modal decomposition methods that are widely applied to study flow dynamics in different applications. The application of POD is primarily limited to flows whose coherent structures can be hierarchically ranked in terms of their energy content. But there are situations when the energy content is not a sufficient criterion to accurately describe the dynamical behavior of the flows. Instead, Koopman Mode Decomposition links the dominant flow features by a representation in the amplitudes-temporal dominant frequencies space.

*Correspondence to: Diana Alina Bistrian, Revolutiei Str. Nr.5, 331128 Hunedoara, Romania.
† diana.bistrian@upt.ro

Current literature has explored a broad variety of applications of ROM. Recently, the POD approach has been incorporated for model order reduction purposes by Chevreuil and Nouy [1], Stefanescu and Navon [2], Dimitriu *et al.* [3], Xiao *et al.* [4], Du *et al.* [5], and Fang *et al.* [6]. POD proved to be an effective technique embedded also in inverse problems, as it was demonstrated by the work of Cao *et al.* [7, 8], Chen *et al.* [9], Stefanescu *et al.* [10], thermal analysis (Bialecki *et al.* [11]), nonlinear structural dynamics problems (Carlberg *et al.* [12]), and aerodynamics (see for reference the recent work of Semaan *et al.* [13]).

In the last decade, Koopman mode theory [14] provided a rigorous theoretical background for global modes analysis, hydrodynamic stability, or triple decomposition in problems describing oscillating phenomena. In 2005, Mezic [15] was the first to discover that normal modes of linear oscillations (which Mezic called *shape modes*) have their natural analogs—Koopman modes—in the context of nonlinear dynamics. The advantage of the shape modes introduced in [15] compared with POD modes is that each shape mode is associated with a pulsation, a growth rate, and each mode has a single distinct frequency. The numerical technique to compute this type of modal decomposition was first introduced in 2008 by Schmid and Sesterhenn [16] and was called dynamic mode decomposition (DMD). The original derivation of DMD in [16] is rooted in the theory of Krylov subspaces [17] as it is classified as an Arnoldi-type method [17]. Only a year later (2009), Rowley *et al.* [18] presented a technique for describing the global behavior of complex nonlinear flows. By decomposing the flow into shape modes determined from spectral analysis of the Koopman operator, they proved the validity of the DMD algorithm of Schmid and Sesterhenn [16] in computation of the shape modes introduced by Mezic in [15].

The theory of Koopman modes decomposition associated with different methods for computing the modes or variants of DMD algorithm was used as a modal decomposition tool in nonlinear dynamics (Schmid *et al.* [19], Schmid [20], and Noack *et al.* [21]) and in fluid mechanics (Rowley *et al.* [22], Frederich and Luchtenburg [23], Bagheri [24], and Alekseev *et al.* [25]) and was recently introduced in turbulent flow problems (Seena and Sung [26] and Hua *et al.* [27]) and also in flow control problems by Bagheri [28] and Brunton *et al.* [29]. For a complete description of the utility of DMD versus POD for model reduction in shallow water problems, the reader is referred to our previous paper (Bistrian and Navon [30]).

The intrusive model order reduction is usually derived by combining the POD and the Galerkin projection methods [30]. This approach suffers from efficiency issues because the Galerkin projection is mathematically performed by laborious calculation and requires stabilization techniques in the process of numerical implementation, as it was argued in [31–35].

To circumvent these shortcomings, we propose in this work a novel approach to derive a nonintrusive reduced order model (NIROM) (i.e., not requiring projecting of the governing equations onto the reduced basis modes) of data originating from Saint-Venant equations [36]) by changing the representation of the system from the state-space representation to the dynamics governed by the linear Koopman operator on two-dimensional (2D) space of observables. The NIROM is computed embedding an adaptive randomized dynamic mode decomposition (ARDMD) to find the reduced basis in the offline stage in association with radial basis function (RBF) 2D interpolation [17] in the online stage to compute the temporal values of the ROM.

Several key innovations are introduced in this paper for the ARDMD-based model order reduction. The first one is represented by the randomization of the numerical data snapshots prior to singular value decomposition (SVD) of matrix data. Thus, we endow the DMD algorithm with a randomized SVD algorithm aiming to improve the accuracy of the reduced order linear model and to reduce the CPU elapsed time. We gain a fast and accurate randomized DMD algorithm, exploiting an efficient low-rank DMD model of input data. The rank of the reduced DMD model represents the unique solution of an optimization problem whose constraints are a sufficiently small relative error of data reconstruction and a sufficiently high correlation coefficient between the numerical data and the DMD solution. We shall refer to this procedure as ARDMD.

The first major advantage of the adaptive randomized DMD proposed in this work is represented by the fact that the algorithm produces a reduced order subspace of Ritz values, having the same dimension as the rank of randomized SVD function. As a consequence, a further selection algorithm of the Ritz values associated with their DMD modes is no longer needed. We employ in the flow

DOI: 10.1002/nme

reconstruction the smallest number of the DMD modes and their amplitudes and Ritz values, respectively, leading to the minimum error of flow reconstruction, because of the adaptive feature of the proposed algorithm. The second major improvement offered by the proposed randomized DMD can be found in the significantly reduction of CPU time for computation of massive numerical data.

A randomized SVD algorithm was recently employed in conjunction with DMD in [37] for processing of high resolution videos in real time. We believe that the present paper is the first work that shows the benefits of an efficient randomized DMD algorithm with application in fluid dynamics.

The Saint-Venant (shallow water) system [36] is employed in the present research to provide the numerical data. The remainder of the article is organized as follows. In Section 2, we recall the principles governing the DMD, and we provide the description of the DMD algorithm employed for decomposition of numerical data. In particular, we discuss the implementation of the randomized DMD for optimal selection of the low-order model rank. Section 3 is dedicated to theoretical considerations about multidimensional RBFs interpolation. A detailed evaluation of the proposed numerical technique is presented in Section 4. Summary and conclusions are drawn in the final section.

2. OFFLINE STAGE: ADAPTIVE RANDOMIZED DYNAMIC MODE DECOMPOSITION FOR NONINTRUSIVE DATA

2.1. Koopman operator—the root of dynamic mode decomposition

Being rooted in the work of French-born American mathematician Bernard Osgood Koopman [14], the Koopman operator is applied to a dynamical system evolving on a manifold $\mathbb{M}$ such that, for all $v_k \in \mathbb{M}$, $v_{k+1} = f(v_k)$, and it maps any scalar-valued function $g : \mathbb{M} \to \mathbb{R}$ into a new function $\mathcal{A}g$ given by

$$\mathcal{A}g(v) = g\left(f(v)\right). \tag{1}$$

It has been demonstrated yet that spectral properties of the flow will be contained in the spectrum of the Koopman operator and even when f is finite-dimensional and nonlinear, the Koopman operator $\mathcal{A}$ is infinite-dimensional and linear [18, [24], 38]. Mezic proved in [15] the unique expansion of each snapshot in terms of vector coefficients ϕ_j that are called Koopman modes (or shape modes) and mode amplitudes $a_j(w)$, such that iterates of v_0 are given by

$$g\left(v_k\right) = \sum_{j=1}^{\infty} \lambda_j^k a_j\left(v_0\right) \phi_j, \quad \lambda_j = e^{\sigma_j + i\omega_j}, \tag{2}$$

where λ_j are called the Ritz eigenvalues of the modal decomposition that are complex-valued flow structures associated with the growth rate σ_j and the frequency ω_j. Koopman modes represent spatial flow structures with time-periodic motion that are optimal in resolving oscillatory behavior. They have been increasingly used because they provide a powerful way of analyzing nonlinear flow dynamics using linear techniques (see, e.g., the work provided by the efforts of Rowley *et al.* [18], Mezic [38], and Bagheri [24]). The Koopman modes are extracted from the data snapshots, and a unique frequency is associated to each mode. This is of major interest for fluid dynamics applications where phenomena occurring at different frequencies must be individualized.

A stable and consistent algorithm introduced in 2008 by Schmid and Sesterhenn [16], referred in the literature as DMD, can be used for computing approximately a subset of the Koopman spectrum from the time series of snapshots of the flow. Thus, DMD generalizes the global stability modes and approximates the eigenvalues of the Koopman operator.

A considerable amount of work has focused on understanding and improving the method of DMD, and several DMD procedures have been released: optimized DMD (Chen *et al.* [39]), exact DMD (Tu *et al.* [40]), sparsity promoting DMD (Jovanovic *et al.* [41]), multi-resolution DMD (Kutz *et al.* [42]), extended DMD (Williams *et al.* [43]), recursive DMD (Noack *et al.* [44]), and DMD with control (Proctor *et al.* [45]). Efficient post processing procedures for selection of the most influential DMD modes and eigenvalues were presented in our previous papers (Bistrian and Navon [30, 46]).

DOI: 10.1002/nme

Employing numerical simulations or experimental measurement techniques, different quantities associated with the flow are measured and collected as observations at one or more time signals, called observables or nonintrusive data. It turns out (see the survey of Bagheri [28]) that monitoring an observable over a very long time interval allows the reconstruction of the flow phase space. Assuming that $\{v_0, v_1, \dots, v_N\}$ is a data sequence collected at a constant sampling time Δt, the DMD algorithm is based on the hypothesis that a Koopman operator $\mathcal{A}$ exists that steps forward in time the snapshots, such that the snapshots data set

$$\left\{v_0,\ \mathcal{A}v_0,\ \mathcal{A}^2v_0,\ \dots,\mathcal{A}^{N-1}v_0\right\} \tag{3}$$

corresponds to the Nth Krylov subspace generated by the Koopman operator from v_0. The goal of DMD is to determine eigenvalues and eigenvectors of the unknown matrix operator $\mathcal{A}$, thus a Galerkin projection of $\mathcal{A}$ onto the subspace spanned by the snapshots is performed. For a sufficiently long sequence of the snapshots, we suppose that the last snapshot v_N can be written as a linear combination of previous $N-1$ vectors, such that

$$v_N = c_0v_0 + c_1v_1 + \cdots + c_{N-1}v_{N-1} + \mathcal{R}, \tag{4}$$

in which c_i, $i = 0, \dots, N-1$ are complex numbers and $\mathcal{R}$ is the residual vector. We assemble the following relations

$$\mathcal{A}\{v_0, v_1, \dots, v_{N-1}\} = \{v_1, v_2, \dots, v_N\} = \left\{v_1, v_2, \dots, V_0^{N-1}c\right\} + \mathcal{R}\mathrm{e}_{N-1}^T, \tag{5}$$

where $V_0^{N-1} = \begin{pmatrix} v_0 & v_1 & \dots & v_{N-1}\end{pmatrix}$, $c^T = \begin{pmatrix} c_0 & c_1 & \dots & c_{N-1}\end{pmatrix}$is the unknown complex column vector, and e_j^T represents the jth Euclidean unitary vector of length $N' - 1$.

In matrix notation form, Equation (5) reads

$$\mathcal{A}V_0^{N-1} = V_0^{N-1}\mathcal{C} + \mathcal{R}\mathrm{e}_{N-1}^T, \quad \mathcal{C} = \begin{pmatrix} 0 & \dots & 0 & c_0 \\ 1 & & 0 & c_1 \\ \vdots & \vdots & \vdots & \vdots \\ 0 & \dots & 1 & c_{N-1} \end{pmatrix}, \tag{6}$$

where $\mathcal{C}$ is the companion matrix [47].

Relation (6) is true when the residual

$$\mathcal{R} = v_N - V_0^{N-1}c \tag{7}$$

is minimized when c is chosen such that $\mathcal{R}$ is orthogonal to $span\{v_0, \dots, v_{N-1}\}$.

A direct consequence of Equation (6) is that decreasing the residual increases overall convergence and therefore the eigenvalues of the companion matrix $\mathcal{C}$ will converge toward the eigenvalues of the Koopman operator $\mathcal{A}$. A detailed spectral analysis of the Koopman operator for linear and nonlinear systems is provided by Rowley *et al.* [18].

The representation of data in terms of DMD is given by

$$v_{DMD}{}^t(\mathbf{x}) = \sum_{j=1}^{k} a_j\phi_j(\mathbf{x})\,\lambda_j^{t-1}, \quad \lambda_j = e^{(\sigma_j + i\omega_j)\Delta t}, \quad t = t_1, \dots, t_N, \tag{8}$$

where the right eigenvectors $\phi_j \in \mathbb{C}$ are dynamic (Koopman) modes, the eigenvalues λ_j are called Ritz values [48], and coefficients $a_j \in \mathbb{C}$ are denoted as amplitudes or Koopman eigenfunctions. Each Ritz value λ_j is associated with the growth rate $\sigma_j = \frac{\log(|\lambda_j|)}{\Delta t}$ and the frequency $\omega_j = \frac{\arg(|\lambda_j|)}{\Delta t}$, and k represents the number of DMD modes involved in reconstruction.

So far, we have noticed two directions in developing the algorithms for DMD. The straight-forward approach proposed by Rowley *et al.* [22] is seeking the companion matrix $\mathcal{C}$ from Equation (6) that helps to construct in a least squares sense the final data vector as a linear combination of all previous data vectors. Because this version may be ill-conditioned in practice, Schmid [20] recommends an alternate algorithm, on the basis of SVD [17] of snapshot matrix, upon which the work within this article is based.

DOI: 10.1002/nme

2.2. *Adaptive randomized dynamic mode decomposition algorithm*

To derive the improved algorithm proposed here, we proceed by collecting data $v_i(t, \mathbf{x}) = v(t_i, \mathbf{x})$, $t_i = i\Delta t$, and $i = 0, \ldots, N$, $\mathbf{x}$ representing the spatial coordinates whether Cartesian or cylindrical and forms the snapshot matrix $V = \begin{bmatrix} v_0 & v_1 & \ldots & v_N \end{bmatrix}$.

We arrange the snapshot matrix into two matrices. A matrix V_0^{N-1} is formed with the first N columns, and the matrix V_1^N contains the last N columns of V: $V_0^{N-1} = \begin{bmatrix} v_0 & v_1 & \ldots & v_{N-1} \end{bmatrix}$, $V_1^N = \begin{bmatrix} v_1 & v_2 & \ldots & v_N \end{bmatrix}$.

Expressing V_1^N as a linear combination of the independent sequence V_0^{N-1} yields

$$V_1^N = \mathcal{A} V_0^{N-1} = V_0^{N-1} \mathcal{S} + R,$$

where R is the residual matrix and $\mathcal{S}$ approximates the eigenvalues of $\mathcal{A}$ when $R_2 \to 0$. The objective at this step is to solve the minimization problem

$$\underset{\mathcal{S}}{Minimize}\, R = V_1^N - V_0^{N-1} \mathcal{S}_2. \tag{9}$$

An estimate can be computed by multiplying V_1^N by the Moore–Penrose pseudoinverse of V_0^{N-1}:

$$\mathcal{S} = \left(V_0^N - 1\right)^+ V_1^N = W \Sigma^+ U^H V_1^N = X \Lambda X^{-1}, \tag{10}$$

where X and Λ represent the eigenvectors, respectively the eigenvalues of $\mathcal{S}$, and Σ^+ is computed according to Moore–Penrose pseudoinverse definition of Golub and van Loan [17]:

$$\Sigma^+ = diag\left(\frac{1}{\sigma_1}, \cdots, \frac{1}{\sigma_r}, 0 \cdots, 0\right), \quad r = rank\left(V_0^{N-1}\right). \tag{11}$$

It can be seen that the SVD plays a central role in computing the DMD. Therefore, the Moore–Penrose pseudoinverse approach we previously employed in [30] might not be feasible when dealing with high-dimensional nonintrusive data. It is more desirable to reduce the problem dimension to avoid a computationally expensive SVD. Several key innovations are introduced in the present paper. The first one is represented by the randomization of data V_0^{N-1} prior to SVD. Thus, we endow the DMD algorithm with a randomized SVD algorithm aiming to improve the accuracy of the reduced order linear model and to reduce the CPU elapsed time. We gain a fast and accurate randomized DMD algorithm, exploiting an efficient low-rank model of input data.

Algorithm 1 describes the procedure for computing the randomized SVD, and it is adapted after Halko *et al.* [49].

Algorithm 1 Randomized SVD algorithm (RSVD)

Initial data: $V_0^{N-1} \in \mathbb{R}^{m \times n}$, $m \geqslant n$, integer target rank $k \geqslant 2$ and $k < n$.

1. Generate random matrix $M = rand(n, r)$, $r = \min(n, 2k)$.
2. Multiplication of snapshot matrix with random matrix $Q = V_0^{N-1} M$.
3. Orthogonalization $Q \leftarrow orth(Q)$.
4. Projection of snapshot matrix $V = Q^H V_0^{N-1}$, where H denotes the conjugate transpose.
5. Produce the economy size singular value decomposition $[Q_1, \Sigma, W] = SVD(V)$.
6. Compute the right singular vectors $U = Q Q_1$.

Output: Procedure returns $U \in \mathbb{R}^{m \times k}$, $\Sigma \in \mathbb{R}^{k \times k}$, $W \in \mathbb{R}^{n \times k}$.

We define the relative error of the low-rank model as the L_2-norm of the difference between the flow variables and approximate DMD solutions over the exact one, that is,

DOI: 10.1002/nme

$$Er_{DMD} = \frac{v(\mathbf{x}) - v_{DMD}(\mathbf{x})_2}{v(\mathbf{x})_2}, \tag{12}$$

where $v(\mathbf{x})$ represents the numerical data and $v_{DMD}(\mathbf{x})$ represents the low-rank DMD approximation.

The correlation coefficient defined next is used as additional metric to validate the quality of the low-rank DMD model:

$$C_{DMD} = \frac{\left(\left\|v(\mathbf{x}) \cdot v_{DMD}(\mathbf{x})\right\|_F\right)^2}{\left\|v(\mathbf{x})^H \cdot v(\mathbf{x})\right\|_F \left\|v_{DMD}(\mathbf{x})^H \cdot v_{DMD}(x)\right\|_F}, \tag{13}$$

where $v(\mathbf{x})$ means the numerical data, $v_{DMD}(x)$ represents the computed solution by means of the reduced order DMD model, $(\cdot)$ represents the Hermitian inner product, and H denotes the conjugate transpose. We denote by $\|\cdot\|_F$ the Frobenius matrix norm in the sense that for any matrix $A \in \mathbb{C}_{m\times n}$ having singular values $\sigma_1, \ldots, \sigma_n$ and SVD of the form $A = U\Sigma V^H$, then

$$\|A\|_F = \left\|U^H A V\right\|_F = \|\Sigma\|_F = \sqrt{{\sigma_1}^2 + \ldots + {\sigma_n}^2}. \tag{14}$$

The rank of the reduced DMD model is given such that the relative error of data reconstruction becomes sufficiently small and the correlation coefficient is sufficiently high. We recall this procedure as *ARDMD*. Determination of the optimal rank of the reduced DMD model then amounts to finding the solution to the following optimization problem:

$$\begin{cases} \underset{k\in\mathbb{N}, k\geqslant 2}{Find} \;\; {v_{DMD}}^t(\mathbf{x}) = \sum_{j=1}^{k} a_j \phi_j(\mathbf{x}) \lambda_j^{t-1}, \\ Subject\ to \;\; k = \arg\min \left\{ Er_{DMD} \leqslant 10^{-3} \; and \; C_{DMD} \geqslant 0.999 \right\}. \end{cases} \tag{15}$$

The adaptive randomized DMD algorithm (**Algorithm 2**) that we applied in the forthcoming section for data originating from the Saint-Venant system proceeds as follows:

In case of the classic DMD algorithm, the superposition of all Koopman modes approximates the entire data sequence, but there are also modes that have a weak contribution. The modes' selection, which is central in model reduction, constitutes the source of many discussions among modal decomposition practitioners (see, for instance, Chen *et al.* [39], Jovanovic *et al.* [50], and Tissot *et al.* [51]). With a conscious effort, we lately investigated different techniques of modes selection in DMD-based ROM.

Reference [30] aimed to present a preliminary survey on DMD modes selection. We proposed a framework for modal decomposition of 2D flows, when numerical data are captured with large time steps. Key innovations for the DMD-based ROM introduced in [30] are the use of the Moore–Penrose pseudoinverse in the DMD computation that produced an accurate result and a novel selection method for the DMD modes. Unlike the classic algorithm, we arrange the Koopman modes in descending order of the energy of the DMD modes weighted by the inverse of the Strouhal number. We eliminate the modes that contribute weakly to the data sequence on the basis of the conservation of quadratic integral invariants [52] by the reduced order flow.

In [25], we proposed a new framework for DMD on the basis of the reduced Schmid operator. We investigated a variant of DMD algorithm, and we explored the selection of the modes on the basis of sorting them in decreasing order of their amplitudes. This procedure works well for models without modes that are very rapidly damped, having very high amplitudes. Therefore, the selection of modes based on their amplitude is effective only in certain situations, as reported also by Noack *et al.* [21].

The investigation we recently presented in [46] has focused on the effects of modes selection in DMD. We proposed a new vector filtering criterion for dynamic modes selection that is able to extract dynamically relevant flow features of time-resolved numerical data. The algorithm related in [46] proposed a dynamic filtering criterion for which the amplitude of any mode is weighted by its growth rate. This method proved to be perfectly adapted to the flow dynamics, in identification of the most influential modes for the investigated problems.

DOI: 10.1002/nme

The first major advantage of the adaptive randomized DMD proposed in this paper is represented by the fact that **Algorithm 2** produces a reduced order subspace of Ritz values, having the same dimension as the rank of randomized SVD algorithm function. In consequence, after solving the optimization problem (15), an additional selection criterion of the Ritz values associated with their DMD modes is no longer needed. We employ in the flow reconstruction the most influential DMD modes associated with their amplitudes and Ritz values, respectively, leading to the minimum error of flow reconstruction, due to the adaptive feature of the proposed algorithm.

Algorithm 2 Adaptive randomized DMD algorithm (ARDMD)

Initial data: $V_0^{N-1} \in \mathbb{R}^{m\times n}$, $V_1^N \in \mathbb{R}^{m\times n}$, $m \geqslant n$, integer target rank $k \geqslant 2$ and $k < n$.

1. For $k = 2$ to $n-1$.
2. Produce the randomized singular value decomposition: $[U, \Sigma, W] = RSVD\left(V_0^{N-1}, k\right)$, where U contains the proper orthogonal modes of V_0^{N-1} and Σ contains the singular values.
3. Solve the minimization problem (9): $S = U^H\left(V_1^N W\Sigma^{-1}\right)$.
   For the reader information we will detail it in the following. Relations $\mathcal{A}V_0^{N-1} = V_1^N = V_0^{N-1}S + R$, $\|R\|_2 \to 0$ and $V_0^{N-1} = U\Sigma W^H$ yield:
$$\begin{aligned} \mathcal{A}U\Sigma W^H = V_1^N &= U\Sigma W^H S \\ \Rightarrow \quad U^H\mathcal{A}U\Sigma W^H &= U^H U\Sigma W^H S \\ \Rightarrow \quad S &= U^H\mathcal{A}U. \end{aligned}$$
   From $\mathcal{A}U\Sigma W^H = V_1^N$ it follows that $\mathcal{A}U = V_1^N W\Sigma^{-1}$ and hence $S = U^H\left(V_1^N W\Sigma^{-1}\right)$.
4. Compute dynamic modes solving the eigenvalue problem $SX = X\Lambda$ and obtain dynamic modes as $\Phi = UX$. The diagonal entries of Λ represent the eigenvalues λ.
5. Project dynamic modes onto the first snapshot to calculate the vector containing dynamic modes amplitudes $Ampl = \left(a_j\right)_{j=1}^{rank(\Lambda)}$.
6. The DMD model of rank k is given by the product
$$V_{DMD} = \Phi \cdot diag(Ampl) \cdot Van, \tag{16}$$
   where the Vandermonde matrix is
$$Van = \begin{pmatrix} 1 & \lambda_1^1 & \lambda_1^2 & \dots & \lambda_1^{N-2} \\ 1 & \lambda_2^1 & \lambda_2^2 & \dots & \lambda_2^{N-2} \\ 1 & \vdots & \vdots & \vdots & \vdots \\ \dots & \dots & \dots & \dots & \dots \\ 1 & \lambda_k^1 & \lambda_k^2 & \dots & \lambda_k^{N-2} \end{pmatrix}.$$
7. Solve the optimization problem (15) and obtain the optimal low-rank k and associated V_{DMD}.
   Output: k, V_{DMD}.

The second major improvement offered by the proposed randomized DMD can be found in the significantly reduction of CPU time for computation of massive numerical data, as we will detail in the section dedicated to numerical results.

3. ONLINE STAGE: INTERPOLATION OF TEMPORAL REDUCED ORDER MODELLING COEFFICIENTS

3.1. Present approach: two-dimensional radial basis function interpolation

Since it was introduced by Rolland Hardy in 1970 [53] for applications in cartography, RBF method has undergone a rapid progress as an active tool of mathematical interpolation of scattered data in

DOI: 10.1002/nme

many application domains like domain decomposition [54], unsteady fluid flows modelling [4, 55], or image processing [56]. Investigations of the accuracy and stability of RBF-based interpolation may be found in Fornberg and Wright [57], Fasshauer [58], and Chenoweth [59].

The ARDMD algorithm previously described allows the identification of a reduced order model of form

$$v_{DMD}{}^{t}(\mathbf{x}) = \sum_{j=1}^{k} a_j \phi_j(\mathbf{x}) \lambda_j^{t-1}, \quad \lambda_j = e^{(\sigma_j + i\omega_j)\Delta t}, \quad t = t_1, \ldots, t_N, \tag{17}$$

in which $\phi_j \in \mathbb{C}$ represents dynamic DMD modes, λ_j are the Ritz values, $a_j \in \mathbb{C}$ represent the modal amplitudes, and k is the truncation order.

In the following, we employ the method of RBF interpolation, as a generalization of Hardy's multiquadric and inverse multiquadric method [60], for numerical interpolation of the model coefficients $b_j{}^t = a_j \lambda_j^{t-1}$ for $t \in [t_1, t_N]$.

Considering the determined coefficients as a set of distinct nodes $\{\boldsymbol{x}_i\}_{i=1}^{k\times N} \subset \mathbb{R}^2$ and a set of function values $\{f_i\}_{i=1}^{k\times N} \subset \mathbb{R}$, the problem reduces to find an interpolant $s : \mathbb{R}^2 \to \mathbb{R}$ such that

$$s(\boldsymbol{x}_i) = f_i \quad for\ i = 1, \ldots, k \times N, \tag{18}$$

where N is the number of time instances for which numerical data are available and k is the number of retained DMD modes. Note that we use the notation $f_i = b_j{}^t, j = 1, \ldots, k, t = t_1, \ldots, t_N$ for scattered points values and $\boldsymbol{x} = (x, y) \in \{1, \ldots, k\} \times [t_1, t_N]$ for scattered points coordinates.

Following Duchon [61] and Green and Silverman [62], we let the RBF interpolant takes the form

$$s(\boldsymbol{x}) = c_0 + c_1 \boldsymbol{x} + \sum_{i=1}^{k\times N} \beta_i K(\boldsymbol{x} - \boldsymbol{x}_i{}_2), \tag{19}$$

where K is a real valued function defined on the kernel $K \in \mathcal{K} : \mathbb{R}^{k\times N} \times \mathbb{R}^{k\times N} \to \mathbb{R}$, $\|\cdot\|_2$ is the Euclidian distance between the points $\boldsymbol{x}$ and $\boldsymbol{x}_i$, and the coefficients $\beta_i \in \mathbb{R}$ are constant real numbers. Following Larsson *et al.* [63], it is beneficial with respect to accuracy and convergence to add the low-order polynomial term $\mathcal{P}(x) = c_0 + c_1 \boldsymbol{x}$, usually considered of small degree, to obtain conditionally positive definite RBFs. The points $\boldsymbol{x}_i$ are referred as centers of the RBFs $K(r) = \mathcal{K}(\boldsymbol{x}, \boldsymbol{x}_i)$, where the variable r stands for $\|\boldsymbol{x} - \boldsymbol{x}_i\|_2$.

The coefficients β_i and the polynomial $\mathcal{P}(x)$ are chosen to satisfy the fitting conditions (18) and the constraints

$$\sum_{i=1}^{k\times N} \beta_i \mathcal{P}(\boldsymbol{x}_i) = 0. \tag{20}$$

Considering that $\{p_1, p_2\}$ represents a basis for the polynomial $\mathcal{P}$ and $\{c_0, c_1\}$ are the coefficients that give the polynomial $\mathcal{P}(\boldsymbol{x})$ in terms of this basis, the interpolation conditions (18) with the constraints (20) lead to the following linear system to be solved for the coefficients that specify the RBF

$$\begin{pmatrix} K & P \\ P^T & 0 \end{pmatrix} \begin{pmatrix} \beta \\ c \end{pmatrix} = \begin{pmatrix} f \\ 0 \end{pmatrix}, \tag{21}$$

where $K_{ij} = K\left(\boldsymbol{x}_i - \boldsymbol{x}_j{}_2\right)$, $i,j = 1, \ldots, k \times N$, $P_{ij} = p_j(\boldsymbol{x}_i)$, $i = 1, \ldots, k \times N$, $j = 1, 2$, $\beta = (\beta_1, \ldots, \beta_{k\times N})^T$, $c = (c_0, c_1)^T$, and $f = (f_1, \ldots, f_{k\times N})^T$. The zeros in Equation (21) denote matrices or vectors of appropriate dimensions, and T stands for the transpose of a matrix or vector. Solving the linear system (21) determines the constant coefficients β and the polynomial coefficients c and hence the interpolant surface $s(\boldsymbol{x})$.

A list of well-known RBF kernels is provided in literature [53, [57]–59] (e.g., *gaussiane*$^{-(r/\sigma)^2}$, *multi-quadratic*$\sqrt{r^2 + \sigma^2}$, and *cubic spliner*^{3}). In this work, the so-called thin-plate kernel $K(r) =$

DOI: 10.1002/nme

$r^2 \ln(r+1)$ is chosen because it ensures that the matrix K in Equation (21) is non-singular and also provides more accurate results than other RBFs, for example, the multi-quadratic and the cubic spline functions, for our test problem.

The methodology presented herein leads to the following linear model (denoted in the following ARDMD−RBF model) for estimation of the flow field for any time instance $t \in [t_1, t_N]$

$$v_{DMD}{}^t(\mathbf{x}) = \sum_{j=1}^{k} b_j{}^t \phi_j(\mathbf{x}), \quad b_j{}^t = s(\boldsymbol{x}_i), \quad \boldsymbol{x}_i \in \{1, \dots, k\} \times [t_1, t_N], \tag{22}$$

where $b_j{}^t$ are the interpolated coefficients, $\phi_j(\mathbf{x})$ are the DMD basis functions, k represents the number of the DMD basis functions retained for the reduced order model, and t denotes any value of time in the interval $[t_1, t_N]$.

3.2. Review of model order reduction using projection and disadvantages

So far, the model order reduction practitioners applied the intrusive model order reduction having modal decomposition (POD or DMD) and the Galerkin projection compound.

In what follows, we consider a coupled system of ordinary differential equations:

$$\begin{cases} \frac{\partial v}{\partial t}(\mathbf{x}, t) = f(t, v(\mathbf{x}, t)), \ t \in (t_0, T] \\ v(\mathbf{x}, t_0) = v_0(\mathbf{x}), \end{cases} \tag{23}$$

where $v_0(\mathbf{x}) \in \mathbb{R}^n$ is a given initial flow and $f : [t_0, T] \times \mathbb{R}^n \to \mathbb{R}^n$ a continuous function in both arguments and locally Lipschitz-type with respect to the second variable. It is well known that under these assumptions, there exists a unique solution for Equation (23).

In the Cartesian or cylindrical coordinates formulation, we suppose there exists the field solution v obtained from the spatial discretization of evolution equations in continuous space. To perform the intrusive model order reduction, we start by replacing the field solution v with reduced order solution v_{DMD} in Equation (23) and project the resulting equations onto the subspace $X^{DMD} = span\{\phi_1(\cdot), \phi_2(\cdot), \dots, \phi_k(\cdot)\}$ spanned by the DMD basis to compute the following inner products:

$$\left\langle \phi_i(\cdot), \sum_{j=1}^{k} \lambda_j \phi_j(\cdot) \dot{a}_j(t) \right\rangle = \left\langle \phi_i(\cdot), f\left(t, \sum_{j=1}^{k} \lambda_j \phi_j(\cdot) a_j(t)\right) \right\rangle, \tag{24}$$

$$\left\langle \phi_i(\cdot), \sum_{j=1}^{k} \lambda_j \phi_j(\cdot) \dot{a}_j(t_0) \right\rangle = \langle \phi_i(\cdot), v_0 \rangle, \text{ for } i = 1, \dots, k, \tag{25}$$

where $\langle f, g \rangle = \int_\Omega fg \, d\Omega$.

The Galerkin projection gives the DMD−ROM, that is, a dynamical system for temporal coefficients $\left\{a_j(t)\right\}_{j=1,\dots,k}$:

$$\dot{a}_i(t) = \left\langle \phi_i(\cdot), f\left(t, \sum_{j=1}^{k} \lambda_j \phi_j(\cdot) a_j(t)\right) \right\rangle, \tag{26}$$

with the initial condition

$$a_i(t_0) = \langle \phi_i(\cdot), v_0 \rangle, \text{ for } i = 1, \dots, k. \tag{27}$$

The resulting autonomous system has linear and quadratic terms parameterized by c_{im}, c_{imn}, respectively:

$$\dot{a}_i(t) = \sum_{m=1}^{k} \sum_{n=1}^{k} c_{imn} a_m(t) a_n(t) + \sum_{m=1}^{k} c_{im} a_m(t), \quad i = 1, \dots, k. \tag{28}$$

DOI: 10.1002/nme

By projecting the full dynamical system onto a reduced space that is constructed on the basis of the optimal DMD basis functions, the computational efficiency can be enhanced by several orders of magnitude [30]. However, this approach presents several shortcomings. As in the case of POD–ROMs [32–[34], [64], 65], the projection method implies analytical calculations, and it remains dependent on the governing equations of the full physical system, therefore is not applicable in case of nonintrusive data. Several techniques to restore the efficiency for nonlinear reduced order models obtained by projection methods are Karhunen–Loeve procedure for gappy data [66] or discrete empirical interpolation [67–69]. In addition, the projection methods require stabilization techniques in the process of numerical implementation, like the ones presented in [31–[35], [69], 70].

In this paper, we propose an efficient approach to derive the reduced order model for nonintrusive data. In the offline stage of the proposed technique, the ARDMD algorithm finds the subspace $X^{DMD} = span\{\phi_1(\cdot), \phi_2(\cdot), \dots, \phi_k(\cdot)\}$ spanned by the sequence of the most efficient DMD modes. In the online stage, we involve the effectual 2D RBF interpolation that elegantly approximates the values of the ROM temporal coefficients. RBFs interpolation proved its efficiency also in POD–ROMs [55, [71], 72].

4. NUMERICAL RESULTS: ANALYSIS OF THE REDUCED ORDER MODEL FOR SAINT-VENANT DATA

4.1. Acquisition of numerical data

The test problem used in this paper is consisting of the nonlinear Saint-Venant equations model (also called the shallow water equations (SWEs) [36]) in a channel on the rotating earth, associated with periodic boundary conditions in the $\tilde{x}$-direction and solid wall boundary condition in the $\tilde{y}$-direction:

$$\tilde{u}_{\tilde{t}} + \tilde{u}\tilde{u}_{\tilde{x}} + \tilde{v}\tilde{u}_{\tilde{y}} + \left(g\tilde{h}\right)_{\tilde{x}} - \tilde{f}\tilde{v} = 0, \tag{29}$$

$$\tilde{v}_{\tilde{t}} + \tilde{u}\tilde{v}_{\tilde{x}} + \tilde{v}\tilde{v}_{\tilde{y}} + \left(g\tilde{h}\right)_{\tilde{y}} + \tilde{f}\tilde{u} = 0, \tag{30}$$

$$\left(g\tilde{h}\right)_{\tilde{t}} + \left(g\tilde{h}\tilde{u}\right)_{\tilde{x}} + \left(g\tilde{h}\tilde{v}\right)_{\tilde{y}} = 0, \tag{31}$$

$$\tilde{u}\left(0, \tilde{y}, \tilde{t}\right) = \tilde{u}\left(L_{\max}, \tilde{y}, \tilde{t}\right), \ \tilde{v}\left(\tilde{x}, 0, \tilde{t}\right) = \tilde{v}\left(\tilde{x}, D_{\max}, \tilde{t}\right) = 0, \tag{32}$$

where $\tilde{u}$ and $\tilde{v}$ are the velocity components in the $\tilde{x}$ and $\tilde{y}$ axis directions, respectively, $g\tilde{h}$ is the geopotential height, $\tilde{h}$ represents the depth of the fluid, $\tilde{f}$ is the Coriolis factor, and g is the acceleration of gravity. We consider that the reference computational configuration is the rectangular 2D domain $\Omega = [0, L_{\max}] \times [0, D_{\max}]$. Subscripts represent the derivatives with respect to time and the streamwise and spanwise coordinates.

The Saint-Venant equations, named after the French mathematician Adhémar Jean Claude Barré de Saint-Venant (1797–1886) (also called in the literature the SWEs), are a set of hyperbolic partial differential equations that describe the flow below a pressure surface in a fluid. A description of the Saint-Venant system has been presented by Vreugdenhil [36], as a result of depth-integration of the Navier–Stokes equations [73]. In the literature, SWEs come up in global atmospheric modelling [74] and are used in various forms to describe hydrological and geophysical fluid dynamics phenomena such as tide–currents [75], pollutant dispersion [76], or tsunami wave propagation [77]. The shallow water magnetohydrodynamic system has been devised by Gilman [78] to analyze the thin-layer evolution of the solar tachocline. Recently, a wave relaxation solver for shallow water magnetohydrodynamic has been developed by Bouchut and Lhébrard [79]. Early work on numerical methods for solving the SWEs is described in Navon (1979) [80].

DOI: 10.1002/nme

We consider the models (29)−(32) in a β-plane assumption detailed in [81], in which the effect of the Earth's sphericity is modeled by a linear variation in the Coriolis factor

$$\tilde{f} = f_0 + \frac{\beta}{2}\left(2\tilde{y} - D_{\max}\right), \tag{33}$$

where f_0,β are constants and $L_{\max}, D_{\max}$ are the dimensions of the rectangular domain of integration.

The following initial condition introduced by Grammeltvedt [82] was adopted as the initial height field that propagates the energy in wave number one, in the streamwise direction:

$$h_0\left(\tilde{x},\tilde{y}\right) = H_0 + H_1 \tanh\left(\frac{9(D_{\max}/2-\tilde{y})}{2D_{\max}}\right) + H_2 \sin\left(\frac{2\pi\tilde{x}}{L_{\max}}\right)\cosh^{-2}\left(\frac{9(D_{\max}/2-\tilde{y})}{D_{\max}}\right). \tag{34}$$

Using the geostrophic relationship $\tilde{u} = -\tilde{h}_{\tilde{y}}\left(g/\tilde{f}\right)$, $\tilde{v} = \tilde{h}_{\tilde{x}}\left(g/\tilde{f}\right)$, the initial velocity fields are derived as

$$u_0\left(\tilde{x},\tilde{y}\right) = -\frac{g}{\tilde{f}}\frac{9H_1}{2D_{\max}}\left(\tanh^2\left(\frac{9D_{\max}/2-9\tilde{y}}{2D_{\max}}\right)-1\right)$$

$$-\frac{18g}{\tilde{f}}H_2 \sinh\left(\frac{9D_{\max}/2-9\tilde{y}}{D_{\max}}\right)\frac{\sin\left(\frac{2\pi\tilde{x}}{L_{\max}}\right)}{D_{\max}\cosh^3\left(\frac{9D_{\max}/2-9\tilde{y}}{D_{\max}}\right)}, \tag{35}$$

$$v_0\left(\tilde{x},\tilde{y}\right) = 2\pi H_2 \frac{g}{\tilde{f}L_{\max}}\cos\left(\frac{2\pi\tilde{x}}{L_{\max}}\right)\cosh^{-2}\left(\frac{9(D_{\max}/2-\tilde{y})}{D_{\max}}\right). \tag{36}$$

The dimensional constants used for the previous test model are

$$f_0 = 10^{-4}s^{-1}, \quad \beta = 1.5\times10^{-11}s^{-1}m^{-1}, \quad g = 10ms^{-1},$$

$$\mathrm{D}_{\max} = 44\times10^5\mathrm{m}, \quad \mathrm{L}_{\max} = 6\times10^6\mathrm{m}, \quad H_0 = 2\times10^6 m, \quad H_1 = 220m, \quad H_2 = 133m. \tag{37}$$

We have followed the approach used by Navon [83], which implements a two-stage finite-element Numerov−Galerkin method for integrating the nonlinear SWEs on a β-plane limited-area domain, for approximating the quadratic nonlinear terms that appear in the equations of hydrological dynamics. This scheme when applied to meteorological and oceanographic problems gives an accurate phase propagation and also handles nonlinearities well. The accuracy of temporal and spatial discretization equals $\mathcal{O}\left(k^2,h^p\right)$, where p varies in the interval [4, 8]. The training data comprise a number of 240 unsteady solutions of the 2D SWEs models (29)−(36), at regularly spaced time intervals $\Delta t = 600$s for each solution variable.

To measure the accuracy of the reduced shallow water model and to validate the numerical results with existing results in the literature, we undertake a nondimensional analysis of the shallow water model. Following [84], reference quantities of the dependent and independent variables in the shallow water model are considered, that is, the length scale $L_{ref} = L_{\max}$ and the reference units for the height and velocity, respectively, are given by the initial conditions $h_{ref} = h_0$, $u_{ref} = u_0$. A typical time scale is also considered, assuming the form $t_{ref} = L_{ref}/u_{ref}$. In order to make the system of Equations (29)−(32) nondimensional, we define the nondimensional variables

$$(t,x,y) = \left(\tilde{t}/t_{ref}, \tilde{x}/L_{ref}, \tilde{y}/L_{ref}\right), \quad (h,u,v) = \left(\tilde{h}/h_{ref}, \tilde{u}/u_{ref}, \tilde{v}/u_{ref}\right). \tag{38}$$

The numerical results are obtained and used in further numerical experiments in dimensionless form.

DOI: 10.1002/nme

4.2. Computational efficiency of adaptive randomized dynamic mode decomposition algorithm

In this section, the efficiency of ROM based on the ARDMD algorithm is illustrated in comparison with the classic DMD algorithm, considering the evolution of the flow field along the integration time window. The first major advantage of the adaptive randomized DMD proposed in this work is represented by the fact that the ARDMD algorithm produces a reduced order subspace of Ritz values, which has the same dimension as the rank of randomized SVD function. In consequence, this

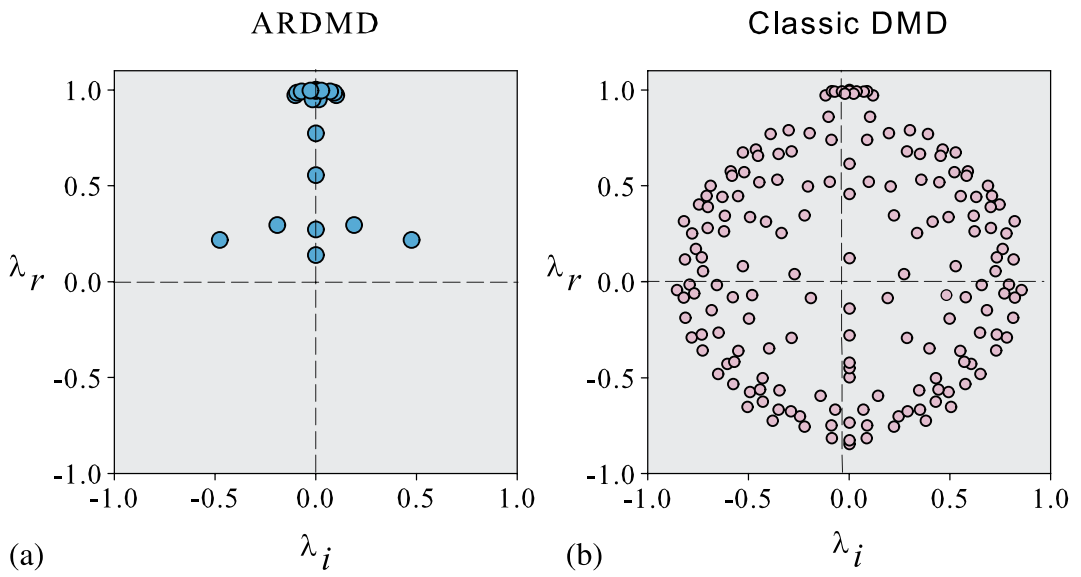

Figure 1. The spectrum of dynamic mode decomposition (DMD) decomposition of geopotential height field h in case of (a) adaptive randomized dynamic mode decomposition (ARDMD) algorithm used in the present paper and (b) classic DMD algorithm used in [46].

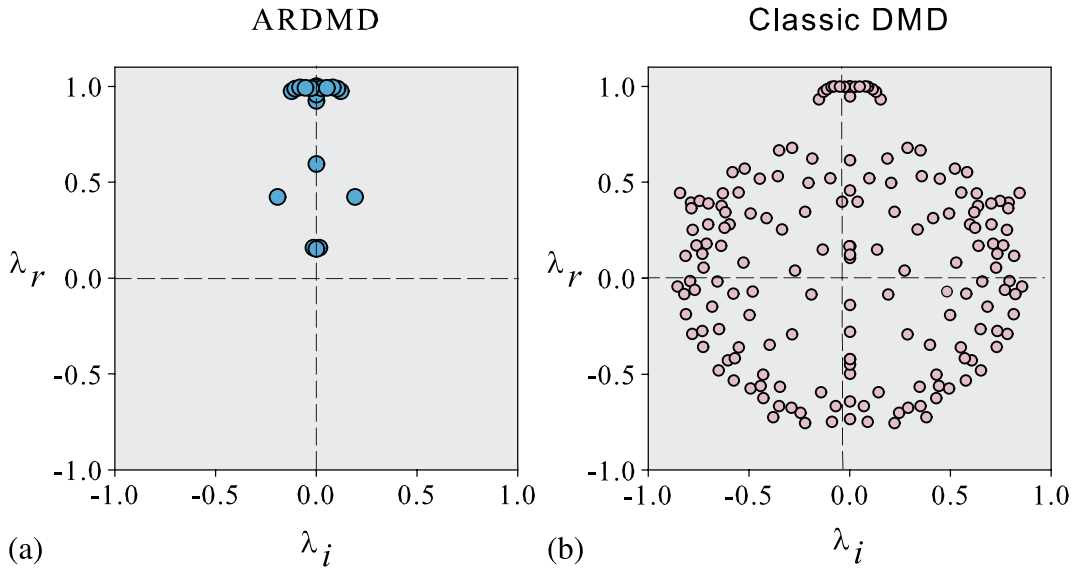

Figure 2. The spectrum of dynamic mode decomposition (DMD) decomposition of streamwise field u in case of (a) adaptive randomized dynamic mode decomposition (ARDMD) algorithm used in the present paper and (b) classic DMD algorithm used in [46].

DOI: 10.1002/nme

procedure omits a further selection procedure of the Ritz values, like those mentioned in literature [21, [25], [30], [39], [46], [50], 51].

Another benefit of the proposed procedure is that the low-order solution (22) is guaranteed to satisfy the boundary conditions (32) of the full model, because the DMD modes provided by the ARDMD algorithm meet the relations

$$\phi_j^u(0,y) = \phi_j^u(L_{\max},y),\ j=1,\ \dots\ ,k, \tag{39}$$

$$\phi_j^v(x,0) = \phi_j^v(x,D_{\max}) = 0,\ j=1,\ \dots\ ,k, \tag{40}$$

where ϕ_j^u, ϕ_j^v are dynamic modes of the u and v fields, respectively, and k represents the number of the retained modes in the ROM.

To highlight the efficiency of the ARDMD method presented herein, we illustrate in Figures 1 –3 the spectra of DMD decomposition of geopotential height field h, streamwise field u, and spanwise

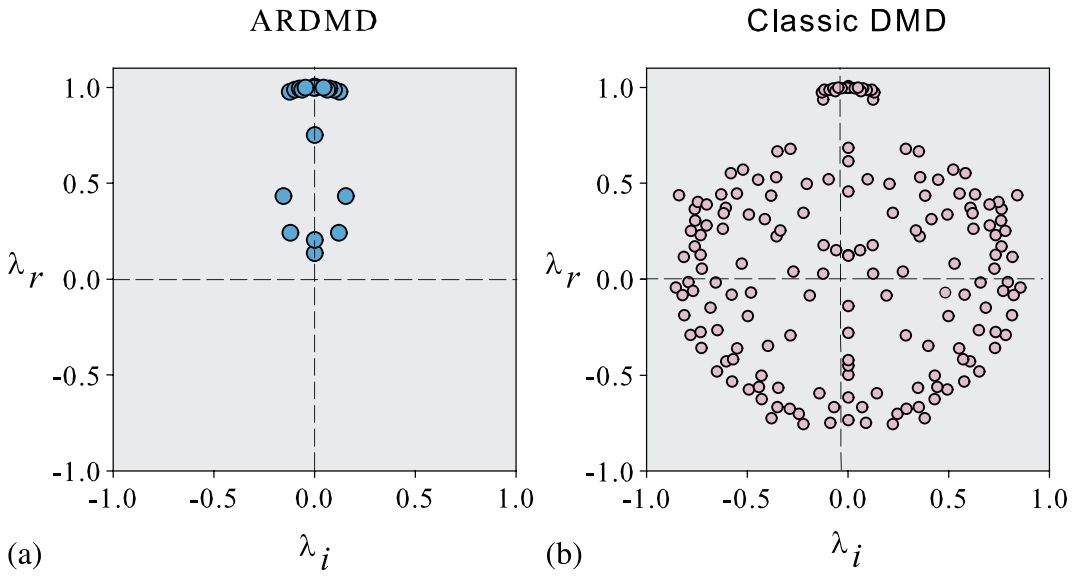

Figure 3. The spectrum of dynamic mode decomposition (DMD) decomposition of spanwise field v in case of (a) adaptive randomized dynamic mode decomposition (ARDMD) algorithm used in the present paper and (b) classic DMD algorithm used in [46].

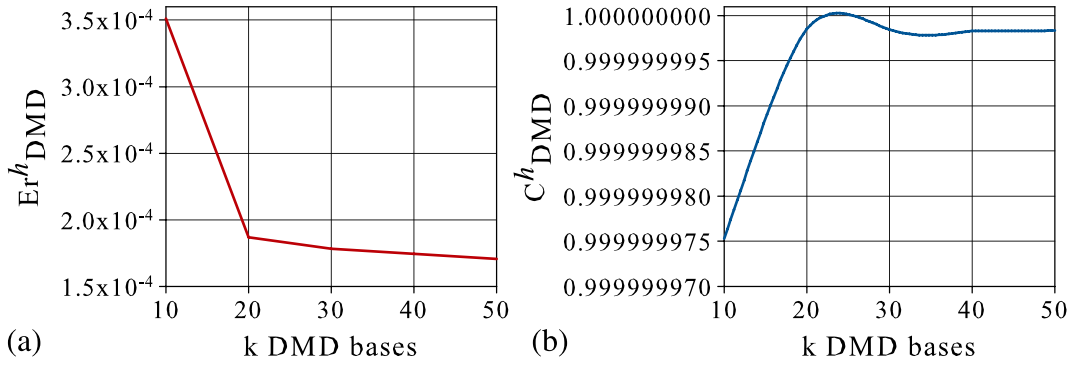

Figure 4. The process of evaluation of ROM target rank for h field: (a) the relative error of ARDMD computed as a function of retained number of dynamic modes, and (b) the correlation coefficient of ARDMD computed as a function of retained number of dynamic modes. ARDMD, adaptive randomized DMD; DMD, dynamic mode decomposition; ROM, reduced order modelling.

DOI: 10.1002/nme

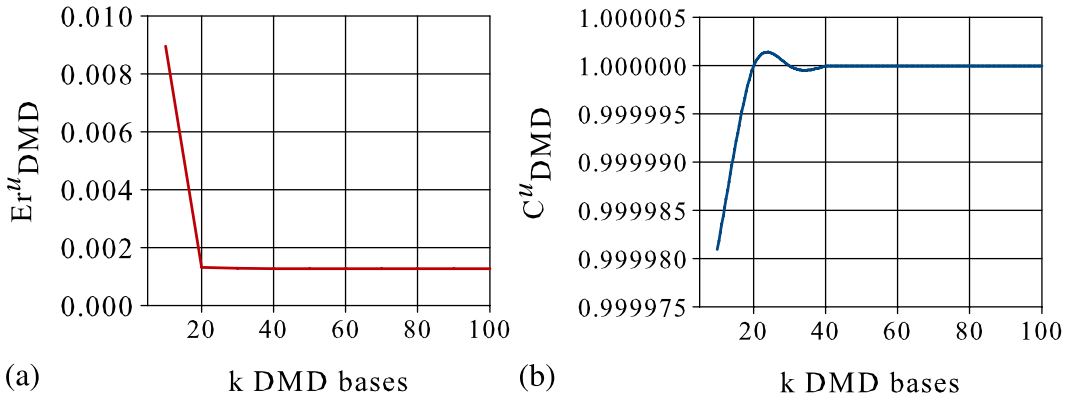

Figure 5. The process of evaluation of ROM target rank for u field: (a) the relative error of ARDMD computed as a function of retained number of dynamic modes, and (b) the correlation coefficient of ARDMD computed as a function of retained number of dynamic modes. ARDMD, adaptive randomized DMD; DMD, dynamic mode decomposition; ROM, reduced order modelling.

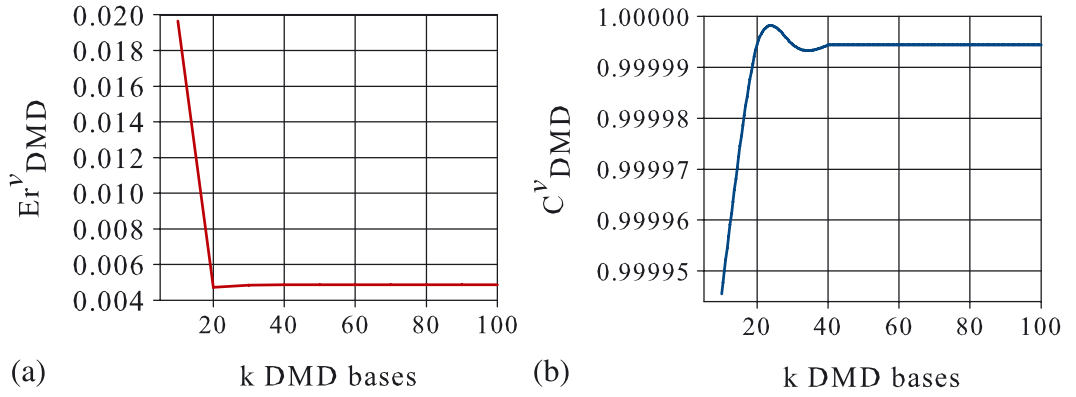

Figure 6. The process of evaluation of ROM target rank for v field: (a) the relative error of ARDMD computed as a function of retained number of dynamic modes, and (b) the correlation coefficient of ARDMD computed as a function of retained number of dynamic modes. ARDMD, adaptive randomized DMD; DMD, dynamic mode decomposition; ROM, reduced order modelling.

field v, respectively, in case of the new ARDMD algorithm and the classic DMD algorithm that was applied in [46].

Obviously, when the classic DMD algorithm is applied, the practitioner has to address a modes' selection method. Instead, the randomized DMD algorithm (ARDMD) produces a significantly reduced size spectrum that elegantly incorporates the most influential modes.

The optimal rank of the reduced DMD model is the unique solution to the optimization problem (15). In the process of ARDMD construction, we have tested several global optimization methods like genetic algorithm combined with sequential quadratic programming [85] and simulated annealing [86], to solve the optimization problem (15), with similar computational difficulties. In this work, a collaborative optimization technique involving hybrid simulated annealing and sequential quadratic programming (SA-SQP-CO) [87] is chosen because it ensures the existence of the solution to the optimization problem (15). The SA-SQP-CO method and its convergence efficiency are fully detailed in [87]. This leads to the optimal low-rank k and associated DMD subspace V_{DMD} where the most influential DMD bases live. The rank of the reduced DMD model is automatically found such that the relative error of field reconstruction given by Equation (12) becomes sufficiently small and the correlation coefficient (13) is sufficiently high.

DOI: 10.1002/nme

Figures 4 –6 present an insight of how ARDMD works. ARDMD algorithm produces subspaces of order $k = 20$ selected from 173 DMD modes. A significant reduction of a factor of eight and a half is achieved for the representation of Saint-Venant fields h, u, and v.

The ARDMD algorithm presented herein is fully capable of determining the modal growth rates and the associated frequencies, which are illustrated in Figure 7 for velocity fields u, v, respectively. This is of major importance when is necessary to isolate modes with very high amplitudes at lower frequencies or high frequency modes having lower amplitudes.

The relative error Er_{DMD}, the correlation coefficient C_{DMD}, and the rank k of reduced order models of the flow fields, provided by the ARDMD algorithm, are presented in Table I.

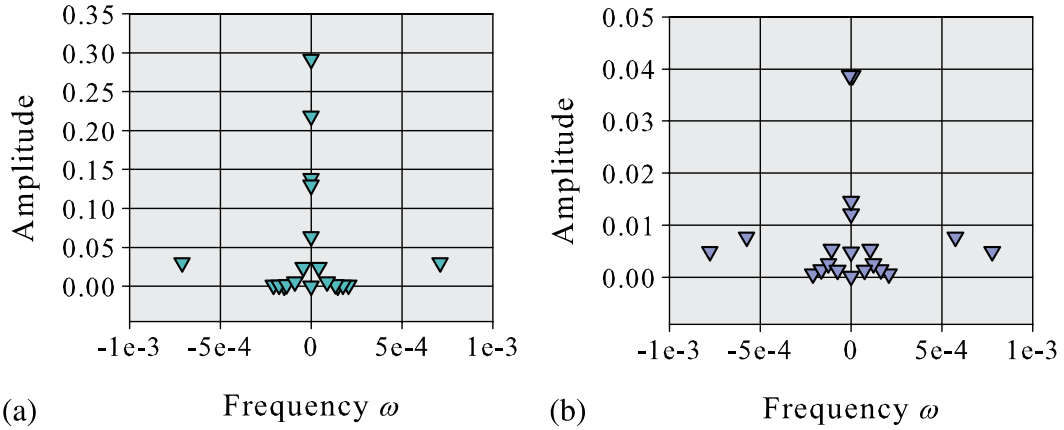

Figure 7. The amplitudes of dynamic mode decomposition modes and associated frequencies obtained by dynamic mode decomposition of (a) streamwise velocity field u and (b) spanwise velocity field v.

Table I. The relative error Er_{DMD}, the correlation coefficient C_{DMD}, and the reduced order modelling rank $k$obtained from ARDMD modal decomposition.

Flow field	The relative error	The correlation coefficient	The ROM rank
$h(x,y)$	$Er^{h}{}_{DMD} = 1.7909 \times 10^{-4}$	$C^{h}{}_{DMD} = 0.99999$	$k = 20$
$u(x,y)$	$Er^{u}{}_{DMD} = 1.4738 \times 10^{-3}$	$C^{u}{}_{DMD} = 0.99999$	$k = 20$
$v(x,y)$	$Er^{v}{}_{DMD} = 4.5316 \times 10^{-3}$	$C^{v}{}_{DMD} = 0.99999$	$k = 20$

ARDMD, adaptive randomized dynamic mode decomposition; ROM, reduced order model.

Table II. The reduced order modelling rank $k$and the relative error $Er^{h}{}_{DMD}$in case of several DMD-based modal decomposition methods.

Energetic DMD [30]	Reduced Schmid operator DMD [25]	Dynamic DMD [46]	ARDMD algorithm the present research
13	19	11	20
1.19×10^{-3}	2.683×10^{-4}	2.5785×10^{-4}	1.7909×10^{-4}

ARDMD, adaptive randomized dynamic mode decomposition; DMD, dynamic mode decomposition.

DOI: 10.1002/nme

A comparison of the ROM rank, in the case of several DMD-based modal decomposition methods associated with different modes' selection criteria proposed in our previous investigations [25, [30], 46], and novel ARDMD technique is presented in Table II.

Data presented in Table II confirms the efficiency of the novel ARDMD method. Although the previous techniques detailed in [25, [30], 46] lead to a reduced number of retained modes, there are still missing modes that would contribute to data approximation. Hence, the relative error of flow reconstruction by the reduced order model is the best in the case of randomized DMD. Producing a slightly larger model rank k than the previous algorithms, the great advantage of ARDMD is that it omits the efforts of implementing an additional criterion of influential modes'selection, they being selected automatically.

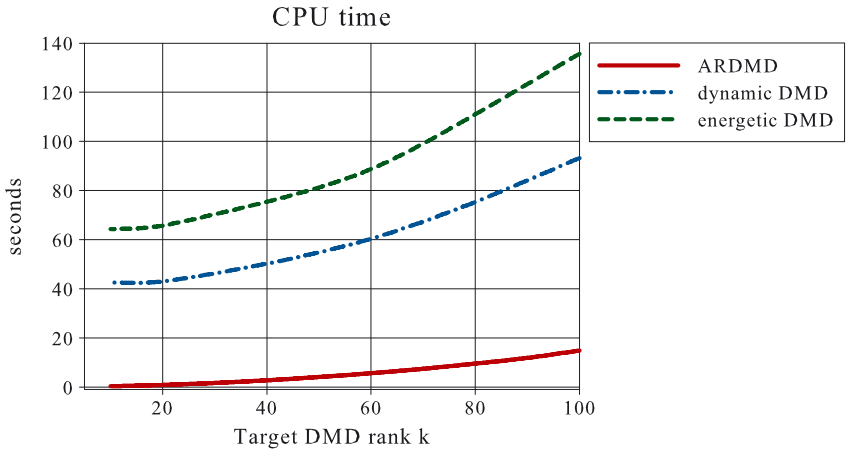

Figure 8. The CPU time required in the offline stage by applying several DMD techniques: ARDMD, adaptive randomized dynamic mode decomposition (present research), dynamic DMD method presented in [46], and energetic DMD method employed in [30].

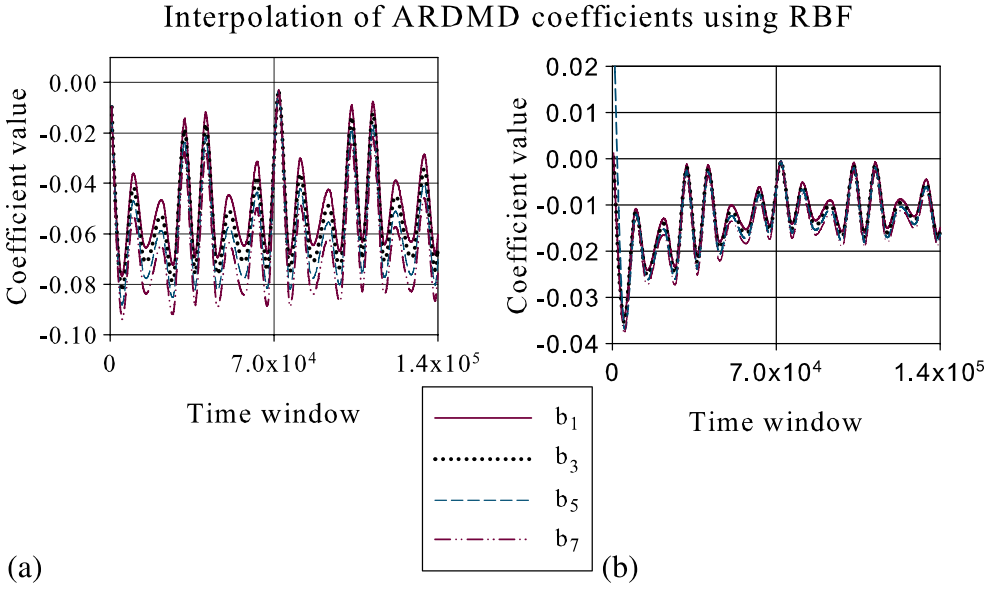

Figure 9. The coefficients of the reduced order models (a) $h_{DMD}(x, y)$ and (b) $u_{DMD}(x, y)$ obtained by radial basis functions (RBF) interpolation, $b_j = a_j \lambda_j^{t-1}$ for $j = 1, \ldots, k$.

DOI: 10.1002/nme

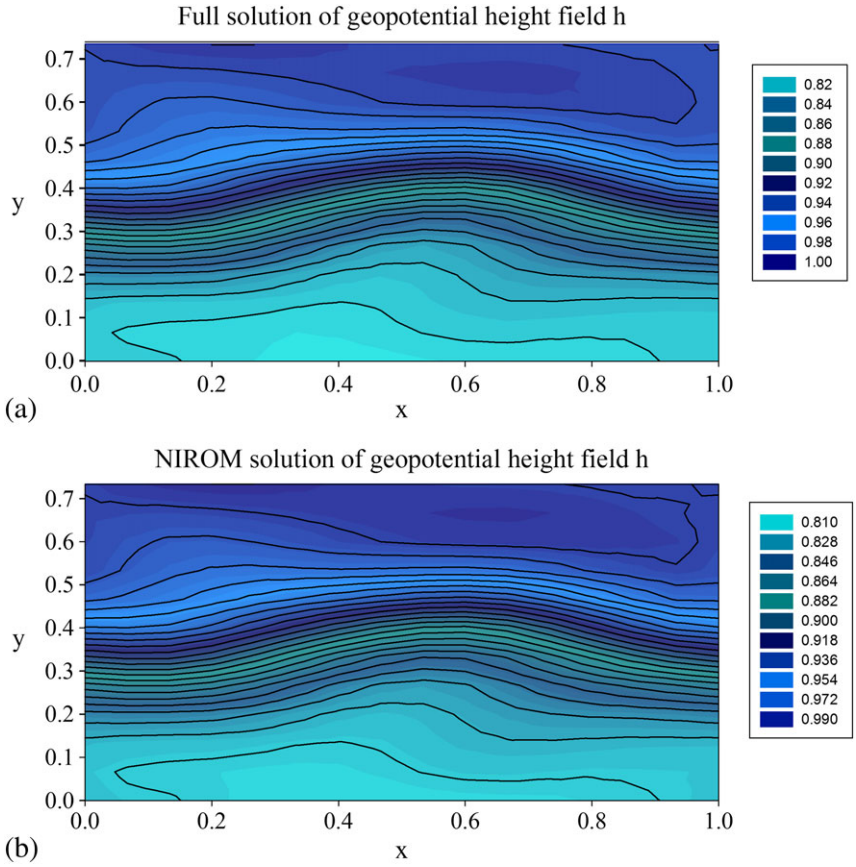

Figure 10. (a) Full solution of geopotential height field; (b) nonintrusive reduced order model (NIROM) solution of geopotential height field.

Thus, a significant reduction in computational time is also achieved comparing with classic DMD associated with different modes selection criteria. The CPU time required in the offline stage is presented in Figure 8. By employing the ARDMD algorithm in comparison with dynamic DMD [46] (DMD associated with a dynamic filtering modes selection method for which the amplitude of any mode is weighted by its growth rate) and energetic DMD [30] (DMD associated with an energetic criterion for modes selection), the computational complexity of the low-order model is reduced from the very beginning by a factor of two and three, respectively, as illustrated in Figure 8.

Estimation of low-order model coefficients by interpolation, in the case of nonintrusive data, represents a cost effective solution, as has been also reported in the literature by Raisee *et al.* [88], Peherstorfer and Willcox [89], and Lin *et al.* [90]. The coefficients of the reduced order models of state solutions $(h_{DMD}, u_{DMD}, v_{DMD})(x, y)$ have been estimated for entire time window by interpolating the DMD computed coefficients using RBFs discussed in Section 3. They are depicted in Figure 9.

Using the ARDMD algorithm, we obtain the NIROMs of the state solutions $(h, u, v)(x, y, t)$. The validity of the methodology introduced in this paper is checked by comparing how the NIROMs assess the full solution fields given by the numerical data at time instance 181, in Figures 10 and 11, respectively. We applied a normalization condition such that the maximum amplitude of the physical components $(h, u, v)(x, y, t)$ fields over the (x, y) stations is unity. The NIROM models employ the Ritz values represented in Figures 1 –3 and associated DMD modes and amplitudes determined by the ARDMD algorithm.

The local error between the full SWE solution and NIROM solution, respectively, at time instance 181 is provided in Figure 12.

DOI: 10.1002/nme

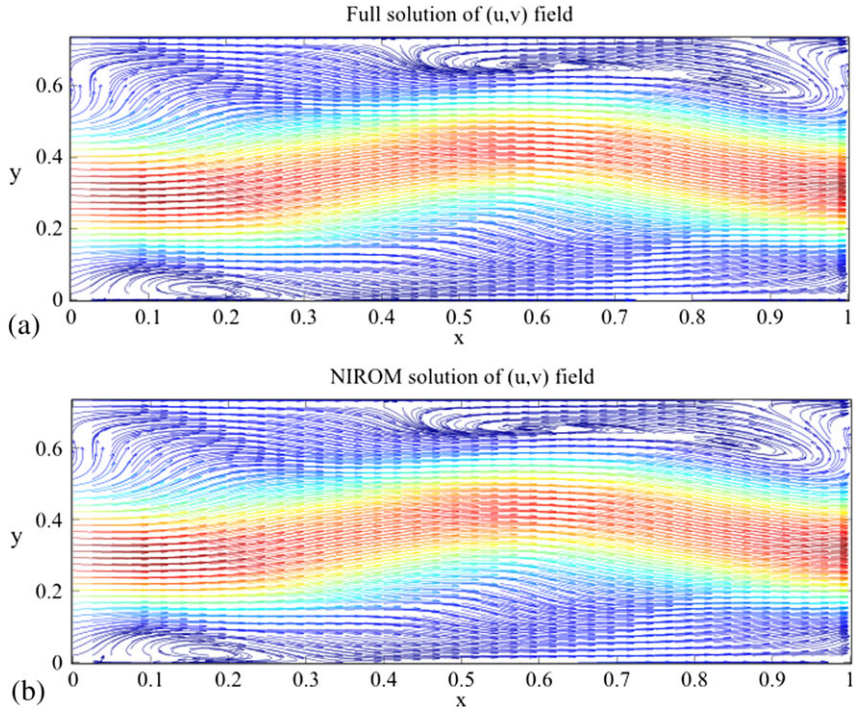

Figure 11. (a) Full solution of (u, v) field; (b) nonintrusive reduced order model (NIROM) solution of (u, v) field.

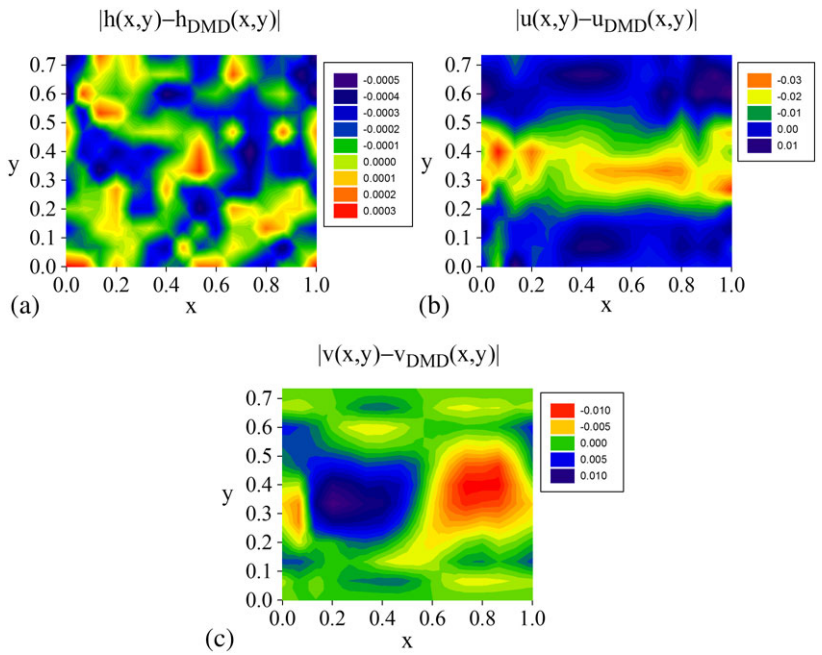

Figure 12. Local error between full shallow water equation solution and nonintrusive reduced order model (NIROM) of geopotential height field (a), NIROM of streamwise velocity field (b), NIROM of spanwise velocity field (c), respectively.

DOI: 10.1002/nme

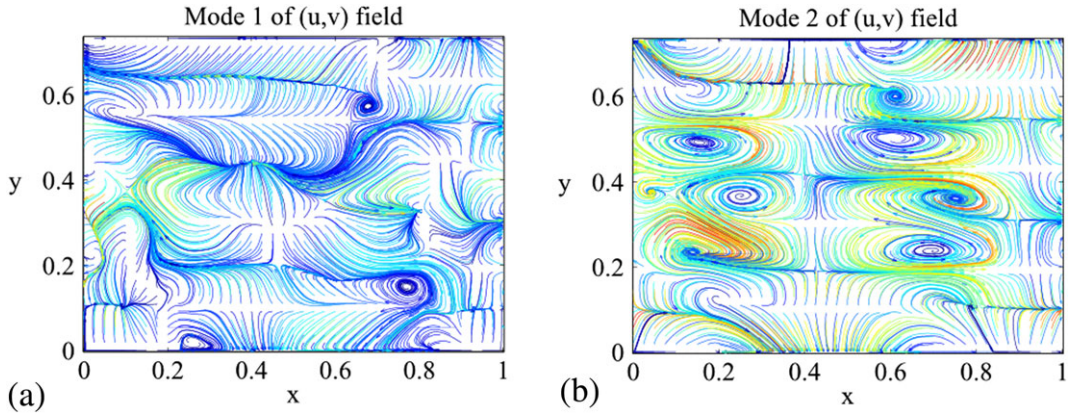

Figure 13. The first two dynamic mode decomposition modes of the (u, v) field.

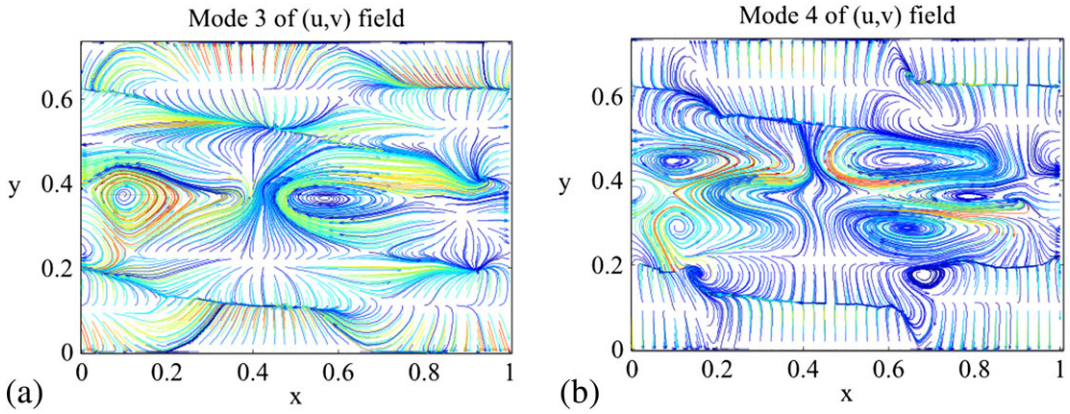

Figure 14. The third and fourth dynamic mode decomposition modes of the (u, v) field.

The coherent structures in the (u, v) field can be visualized as local vortices in the first DMD modes, which are illustrated in Figures 13 and 14.

The flow reconstructions by NIROMs presented in Figures 10 and 11 are very close to numerical data snapshots, comparing the solution of SWE flow field after 181 steps. The values of the correlation coefficients provided in Table I greater than 99% confirm the validity of the NIROMs. The similarity between the characteristics of the flow field and those obtained by the NIROMs validates the method presented here and certifies that the improved ARDMD method can be applied successfully to model reduction of 2D flows.

For the problem investigated here, the novel ARDMD method exhibits satisfactory performances and provides a higher degree of accuracy for our linear reduced order flow model.

5. SUMMARY AND CONCLUSIONS

In this paper, we have proposed a framework for ROM of nonintrusive data with application to 2D flows. To overcome the inconveniences of intrusive model order reduction usually derived by combining the POD and the Galerkin projection methods, we developed a novel technique on the basis of randomized DMD as a fast and accurate option in model order reduction of nonintrusive data originating from Saint-Venant systems. We derived a nonintrusive approach to obtain a reduced order linear model of the flow dynamics on the basis of DMD of numerical data in association with the efficient RBF interpolation technique.

DOI: 10.1002/nme

To the best of our knowledge, the present paper is the first work that introduces the randomized DMD algorithm with application to fluid dynamics, after the randomized SVD algorithm recently introduced by Erichson and Donovan [37] for processing of high resolution videos.

Several key innovations have been introduced in the present paper:

- We endow the DMD algorithm with a randomized singular value decomposition algorithm.
- We gain a fast and accurate ARDMD algorithm, exploiting an efficient low-rank DMD model of input data.
- The rank of the reduced DMD model is given as the unique solution of an optimization problem whose constraints are a sufficiently small relative error of data reconstruction and a sufficiently high correlation coefficient between the numerical data and the DMD solution. The optimization problem (15) is solved using an SA-SQP-CO [87].

The major advantages of the ARDMD proposed in this work are the following:

- This method provides an efficient tool in developing the linear model of a complex flow field described by nonintrusive data.
- This method does not require an additional selection algorithm of the DMD modes. ARDMD produces a reduced order subspace of Ritz values, having the same dimension as the rank of randomized SVD function, where the most influential DMD modes live.
- The low-order solution (22) is guaranteed to satisfy the boundary conditions (32) of the full model.
- We gain a significantly reduction of the offline CPU time in computation of the ROM compared with classic DMD associated with different modes selection criteria.
- Combining the randomized DMD with RBF interpolation, we have derived a reduced order model for estimating the flow behavior in the real-time window. The NIROM presents satisfactory performances in flow reconstruction.
- Analyzing the modal growth rates and the associated frequencies is an instance of capturing the flow dynamics. This is of major importance when is necessary to isolate modes with very high amplitudes at lower frequencies or high frequency modes having lower amplitudes. Thus, this paper outlines steps toward hydrodynamic stability analysis and flow control with potential applications.

To highlight the performances of the proposed methodology, we performed a comparison of the ROM rank, in the case of several DMD-based modal decomposition methods associated with different modes selection criteria and novel ARDMD technique presented herein. The numerical results confirmed the efficiency of the novel ARDMD method.

We emphasized the excellent behavior of the NIROMs developed in this paper by comparing the computed shallow water solution with the numerical flow fields, and we found a close agreement. In addition, we performed a qualitative analysis of the reduced order models by correlation coefficients and local errors.

There are a number of interesting directions that arise from this work. First, it will be a natural extension to apply the proposed algorithm to high-dimensional data originating from fluid dynamics and oceanographic/atmospheric measurements. The methodology presented here offers the main advantage of deriving a reduced order model capable to provide a variety of information describing the behavior of the flow field. A future extension of this research will address an efficient numerical approach for modal decomposition of swirling flows, where the full mathematical model implies more sophisticated relations at domain boundaries that must be satisfied by the reduced order model also. Moreover, the approach presented here (i.e., modal decomposition based on the randomized SVD algorithm) can be used also with other reduced bases not just DMD ones, for example, POD or balanced POD bases. The application of an adaptive randomized POD–ROM strategy for nonintrusive ROM represents a subject that we will further address in our studies.

DOI: 10.1002/nme

ACKNOWLEDGMENTS

The authors would like to thank Igor Mezic for insightful and constructive comments on an early draft of this paper. We also thank the anonymous reviewers who greatly contributed in improving the presentation of the present paper.

REFERENCES

1. Chevreuil M, Nouy A. Model order reduction based on proper generalized decomposition for the propagation of uncertainties in structural dynamics. *International Journal for Numerical Methods in Engineering* 2011; **89**(2):241–268.
2. Stefanescu R, Navon IM. POD/DEIM nonlinear model order reduction of an ADI implicit shallow water equations model. *Journal of Computational Physics* 2013; **237**:95–114.
3. Dimitriu G, Stefanescu R, Navon IM. POD–DEIM approach on dimension reduction of a multi-species host-parasitoid system. *Annals of the Academy of Romanian Scientists, Mathematics and Its Applications* 2015; **7**(1):173–188.
4. Xiao D, Fang F, Pain C, Hu G. Non-intrusive reduced-order modelling of the Navier–Stokes equations based on RBF interpolation. *International Journal for Numerical Methods in Fluids* 2015; **79**(11):580–595.
5. Du J, Fang F, Pain CC, Navon IM, Zhu J, Ham D. POD reduced order unstructured mesh modelling applied to 2D and 3D fluid flow. *Computers and Mathematics with Applications* 2013; **65**:362–379.
6. Fang F, Pain CC, Navon IM, Cacuci DG, Chen X. The independent set perturbation method for efficient computation of sensitivities with applications to data assimilation and a finite element shallow water model. *Computers and Fluids* 2013; **76**:33–49.
7. Cao Y, Zhu J, Luo Z, Navon IM. Reduced order modeling of the upper tropical Pacific ocean model using Proper Orthogonal Decomposition. *Computers and Mathematics with Applications* 2006; **52**(8-9):1373–1386.
8. Cao Y, Zhu J, Navon I, Luo Z. A reduced order approach to four-dimensional variational data assimilation using Proper Orthogonal Decomposition. *International Journal for Numerical Methods in Fluids* 2007; **53**(10):1571–1583.
9. Chen X, Navon IM, Fang F. A dual-weighted trust-region adaptive POD 4D-VAR applied to a finite-element shallow-water equations model. *International Journal for Numerical Methods in Fluids* 2011; **65**:250–541.
10. Stefanescu R, Sandu A, Navon IM. POD/DEIM reduced-order strategies for efficient four dimensional variational data assimilation. *Journal of Computational Physics* 2015; **295**:569–595.
11. Bialecki RA, Fic AJKA. Proper Orthogonal Decomposition and modal analysis for acceleration of transient FEM thermal analysis. *International Journal for Numerical Methods in Engineering* 2004; **62**(6):774–797.
12. Carlberg K, Bou-Mosleh C, Farhat C. Efficient non-linear model reduction via a least-squares Petrov–Galerkin projection and compressive tensor approximations. *International Journal for Numerical Methods in Engineering* 2011; **86**(2):155–181.
13. Semaan R, Kumar P, Burnazzi M, Tissot G, Cordier L, Noack BR. Reduced-order modelling of the flow around a high-lift configuration with unsteady Coanda blowing. *Journal of Fluid Mechanics* 2016; **800**:72–110.
14. Koopman B. Hamiltonian systems and transformations in Hilbert space. *Proceedings of the National Academy of Sciences* 1931; **17**:315–318.
15. Mezic I. Spectral properties of dynamical systems, model reduction and decompositions. *Nonlinear Dynamics* 2005; **41**(1-3):309–325.
16. Schmid PJ, Sesterhenn J. Dynamic mode decomposition of numerical and experimental data. In *61st Annual Meeting of the APS Division of Fluid Dynamics*, vol. 53(15). American Physical Society: San Antonio, Texas, 2008.
17. Golub G, van Loan CF. *Matrix Computations* (3rd edn.) The Johns Hopkins University Press: Baltimore and London, 1996.
18. Rowley CW, Mezic I, Bagheri S, Schlatter P, Henningson DS. Spectral analysis of nonlinear flows. *Journal of Fluid Mechanics* 2009; **641**:115–127.
19. Schmid PJ, Meyer KE, Pust O. Dynamic mode decomposition and Proper Orthogonal Decomposition of flow in a lid-driven cylindrical cavity. In *8th International Symposium on Particle Image Velocimetry - PIV09*, Melbourne, Victoria, Australia, August 25–28, 2009.
20. Schmid P. Dynamic mode decomposition of numerical and experimental data. *Journal of Fluid Mechanics* 2010; **656**:5–28.
21. Noack BR, Morzynski M, Tadmor G. *Reduced-order Modelling for Flow Control*. Springer-Verlag: Wien, 2011.
22. Rowley CW, Mezic I, Bagheri S, Schlatter P, Henningson DS. Reduced-order models for flow control: balanced models and Koopman modes. *Seventh IUTAM Symposium on Laminar-Turbulent Transition, IUTAM Bookseries* 2010; **18**:43–50.
23. Frederich O, Luchtenburg DM. Modal analysis of complex turbulent flow. In *The 7th International Symposium on Turbulence and Shear Flow Phenomena (TSFP-7)*: Ottawa, Canada, 2011; 1–6.
24. Bagheri S. Koopman-mode decomposition of the cylinder wake. *Journal of Fluid Mechanics* 2013; **726**:596–623.
25. Alekseev AK, Bistrian DA, Bondarev AE, Navon IM. On linear and nonlinear aspects of dynamic mode decomposition. *International Journal for Numerical Methods in Fluids* 2016; **82**:348–371, 10.1002/fld.4221.
26. Seena A, Sung HJ. Dynamic mode decomposition of turbulent cavity flows for self-sustained oscillations. *International Journal of Heat and Fluid Flow* 2011; **32**:1098–1110.
27. Hua JC, Gunaratne GH, Talley DG, Gord JR, Roy S. Dynamic-mode decomposition based analysis of shear coaxial jets with and without transverse acoustic driving. *Journal of Fluid Mechanics* 2016; **790**:5–32.

DOI: 10.1002/nme

28. Bagheri S. Computational hydrodynamic stability and flow control based on spectral analysis of linear operators. *Archives of Computational Methods in Engineering* 2012; **19**(3):341–379.
29. Brunton SL, Brunton BW, Proctor JL, Kutz JN. Koopman invariant subspaces and finite linear representations of nonlinear dynamical systems for control. *PLoS ONE* 2016; **11**(2):e0150171, 10.1371/journal.pone.0150171.
30. Bistrian DA, Navon IM. An improved algorithm for the shallow water equations model reduction: dynamic mode decomposition vs POD. *International Journal for Numerical Methods in Fluids* 2015; **78**(9):552–580.
31. Barone MF, Kalashnikova I, Segalman DJ, Thornquist H. Stable Galerkin reduced order models for linearized compressible flow. *Journal of Computational Physics* 2009; **288**:1932–1946.
32. Amsallem D, Farhat C. Stabilization of projection-based reduced-order models. *International Journal for Numerical Methods in Engineering* 2011; **91**(4):358–377.
33. San O, Iliescu T. A stabilized Proper Orthogonal Decomposition reduced-order model for large scale quasigeostrophic ocean circulation. *Advances in Computational Mathematics* 2014; **41**(5):1289–1319.
34. Ballarin F, Manzoni A, Quarteroni A, Rozza G. Supremizer stabilization of POD-Galerkin approximation of parametrized steady incompressible Navier–Stokes equations. *International Journal for Numerical Methods in Engineering* 2015; **102**(5):1136–1161.
35. Balajewicz M, Tezaur I, Dowell E. Minimal subspace rotation on the Stiefel manifold for stabilization and enhancement of projection–based reduced order models for the compressible Navier–Stokes equations. *Journal of Computational Physics* 2016; **321**:224–241.
36. Vreugdenhil C. *Numerical Methods for Shallow Water Flow*. Kluwer Academic Publishers: Dordrecht, Boston, 1994.
37. Erichson NB, Donovan C. Randomized low-rank dynamic mode decomposition for motion detection. *Computer Vision and Image Understanding* 2016; **146**:40–50.
38. Mezic I. Analysis of fluid flows via spectral properties of the Koopman operator. *Annual Review of Fluid Mechanics* 2013; **45**(1):357–378.
39. Chen KK, Tu JH, Rowley CW. Variants of dynamic mode decomposition: boundary condition, Koopman and Fourier analyses. *Nonlinear Science* 2012; **22**:887–915.
40. Tu JH, Rowley CW, Luchtenburg DM, Brunton SL, Kutz JN. On dynamic mode decomposition: theory and applications. *Journal of Computational Dynamics* 2014; **1**(2):391–421.
41. Jovanovic MR, Schmid PJ, Nichols JW. Sparsity-promoting dynamic mode decomposition. *Physics of Fluids* 2014; **26**:024103-1-22.
42. Kutz JN, Fu X, Brunton SL, Erichson NB. Multi-resolution dynamic mode decomposition for foreground/background separation and object tracking. In *2015 IEEE International Conference on Computer Vision Workshop (ICCVW), INSPEC Accession Number:15790263*, IEEE: Santiago, 2015; 921–929.
43. Williams MO, Kevrekidis IG, Rowley CW. A data-driven approximation of the Koopman operator: extending dynamic mode decomposition. *Nonlinear Science* 2015; **25**(6):1307–1346, 10.1007/s00332-015-9258-5.
44. Noack BR, Stankiewicz W, Morzynski M, Schmid PJ. Recursive dynamic mode decomposition of transient and post-transient wake flows. *Journal of Fluid Mechanics* 2016; **809**:843–872.
45. Proctor JL, Brunton SL, Kutz JN. Dynamic mode decomposition with control. *SIAM Journal of Applied Dynamical Systems* 2016; **15**(1):142–161.
46. Bistrian DA, Navon IM. The method of dynamic mode decomposition in shallow water and a swirling flow problem. *International Journal for Numerical Methods in Fluids* 2017; **83**:73–89, 10.1002/fld.4257.
47. Fiedler M. A note on companion matrices. *Linear Algebra and its Applications* 2003; **372**:325–331.
48. Chopra AK. *Dynamics of Structures* (4th edn.) Prentice-Hall International Series in Civil Engineering and Engineering Mechanics: New Jersey, 2000.
49. Halko N, Martinsson PG, Tropp JA. Finding structure with randomness: probabilistic algorithms for constructing approximate matrix decompositions. *SIAM Review* 2011; **53**(2):2017–288.
50. Jovanovic MR, Schmid PJ, Nichols JW. Low-rank and sparse dynamic mode decomposition. *Center for Turbulence Research Annual Research Briefs* 2012:139–152.
51. Tissot G, Cordier L, Benard N, Noack BR. Model reduction using dynamic mode decomposition. *Comptes Rendus Mecanique* 2014; **342**:410–416.
52. Navon IM, DeVilliers R, Gustaf R. A quasi-Newton nonlinear ADI Fortran IV program for solving the shallow-water equations with augmented Lagrangians. *Computers and Geosciences* 1986; **12**:151–173.
53. Hardy RL. Multiquadric equations of topography and other irregular surfaces. *Journal of Geophysical Research* 1970; **76**(8):1905–1915.
54. Beatson RK, Light WA, Billings S. Fast solution of the radial basis function interpolation equations: domain decomposition methods. *SIAM Journal of Scientific Computing* 2000; **22**(5):1717–1740.
55. Walton S, Hassan O, Morgan K. Reduced order modelling for unsteady fluid flow using Proper Orthogonal Decomposition and radial basis functions. *Applied Mathematical Modelling* 2013; **37**:8930–8945.
56. Carr JC, Beatson RK, Cherrie JB, Mitchell TJ, Fright WR, McCallum BC, Evans TR. Reconstruction and representation of 3D objects with radial basis functions. *ACM SIGGRAPH* 2001; **2001**:67–76.
57. Fornberg B, Wright G. Stable computation of multiquadric interpolants for all values of the shape parameter. *Computers and Mathematics with Applications* 2004; **48**:853–867.
58. Fasshauer GE. *Meshfree Approximation Methods with MATLAB*. World Scientific Publishers: Singapore, 2007.
59. Chenoweth ME. A numerical study of generalized mutliquadric radial basis function interpolation. *SIAM Undergraduate Research Online* 2009; **2**:58–70.

DOI: 10.1002/nme

60. Hardy RL. Theory and applications of the multiquadric-biharmonic method: 20 years of discovery. *Computers and Mathematics with Applications* 1990; **19**:163–208.
61. Duchon J. In *Constructive theory of functions of several variables*, vol. Lecture Notes in Mathematics, chap. Splines minimizing rotation-invariant semi-norms in Sobolev spaces Springer-Verlag, Berlin, Heidelberg; 85–100, 1977.
62. Green PJ, Silverman BW. *Nonparametric Regression and Generalized Linear Models: A Roughness Penalty Approach* (1st edn.) Chapman and Hall/CRC: London, 1993.
63. Larsson E, Lehto E, Heryudono A, Fornberg B. Stable computation of differentiation matrices and scattered node stencils based on gaussian radial basis functions. *SIAM Journal on Scientific Computing* 2013; **35**(4):A2096–A2119.
64. Xiao D, Lin Z, Fang F, Pain CC, Navon IM, Salinas P, Muggeridge A. Non-intrusive reduced-order modeling for multiphase porous media flows using Smolyak sparse grids. *International Journal for Numerical Methods in Fluids* 2017; **83**:205–219, 10.1002/fld.4263.
65. Dehghan M, Mohammadi V. Two numerical meshless techniques based on radial basis functions (RBFs) and the method of generalized moving least squares (GMLS) for simulation of coupled Klein–Gordon–Schrodinger (KGS) equations. *Computers and Mathematics with Applications* 2016; **71**:892–921.
66. Everson R, Sirovich L. Karhunen–Loeve procedure for gappy data. *Journal of the Optical Society of America A* 1995; **12**(8):1657–1664.
67. Chaturantabut SD, Sorensen D. Nonlinear model reduction via discrete empirical interpolation. *SIAM Journal on Scientific Computing* 2010; **32**:2737–2764.
68. Dimitriu G, Navon IM, Stefanescu R. Application of a POD–DEIM approach for dimension reduction of a diffusive predator–prey system with Allee effect. *Lecture Notes in Computer Science, Large-Scale Scientific Computing* 2014; **LNCS 8353**(42):373–381.
69. Wang Y, Navon IM, Wang X, Cheng Y. 2D Burgers Equation with Large Reynolds Number Using POD/DEIM and Calibration. *International Journal for Numerical Methods in Fluids* 2016; **82**(12):909–931.
70. Maday Y, Manzoni A, Quarteroni A. An online intrinsic stabilization strategy for the reduced basis approximation of parametrized advection-dominated problems. *Comptes Rendus de l'Académie des Sciences - Series I* 2016; **354**:1188–1194.
71. Bistrian DA, Susan-Resiga RF. Weighted Proper Orthogonal Decomposition of the swirling flow exiting the hydraulic turbine runner. *Applied Mathematical Modelling* 2016; **40**:4057–4078.
72. Xiao D, Yang P, Fang F, Pain CC, Navon IM. Non-intrusive reduced order modelling of fluid structure interactions. *Computer Methods in Applied Mechanics and Engineering* 2016; **303**:35–54.
73. Galdi G. *An Introduction to the Mathematical Theory of the Navier–Stokes Equation*. Springer-Verlag: New York, 1994.
74. Williamson DL, Drake JB, Hack JJ, Jakob R, Swarztrauber PN. A standard test set for numerical approximations of the shallow water equations in spherical geometry. *Journal of Computational Physics* 1992; **102**:211–224.
75. Bryden IG, Couch SJ, Owen A, Melville G. Tidequations resource assessment. *Proc. IMechE Part A: Journal of Power and Energy* 2007; **221**:125–135.
76. Sportisse B, Djouad R. Reduction of chemical kinetics in air pollution modeling. *Journal of Computational Physics* 2000; **164**:354–376.
77. Koutitus C. *Mathematics Models in Coastal Engineering*. Pentech Press: London, 1988.
78. Gilman P. Magnetohydrodynamic "shallow water" equations for the solar tachocline. *The Astrophysical Journal Letters* 2000; **554**:L79–L82.
79. Bouchut F, Lhebrard X. A 5-wave relaxation solver for the shallow water MHD system. *Journal of Scientific Computing* 2016; **68**:92–115.
80. Navon IM. Finite-element simulation of the shallow-water equations model on a limited area domain. *Applied Mathematical Modeling* 1979; **3**:337–348.
81. Navon IM. A Numerov–Galerkin technique applied to a finite-ement shallow water equations model with enforced conservation of integral invariants and selective lumping. *Journal of Computational Physics* 1983; **52**:313–339.
82. Grammeltvedt A. A survey of finite-diference schemes for the primitive equations for a barotropic fluid. *Monthly Weather Review* 1969; **97**(5):384–404.
83. Navon IM. FEUDX: a two-stage, high accuracy, finite-element Fortran program for solving shallow-water equations. *Computers and Geosciences* 1987; **13**(3):255–285.
84. Barenblatt GI. *Scaling, Self-similarity and Intermediate Asymptotics. Cambridge Texts in Applied Mathematics*. Cambridge University Press: Cambridge, New York, Melbourne, 1996.
85. Nocedal J, Wright SJ. *Numerical Optimization* (2nd edn.) Springer-Verlag: New York, 2006.
86. Yang XS. *Engineering Optimization: An Introduction with Metaheuristic Applications*. Wiley: USA, 2010.
87. Cao L, Chen Z, Jiang P, Zhou Q, Zhou H. Collaborative optimization using hybrid simulated annealing optimization and sequential quadratic programming. In *Proceedings of the 14th IFToMM World Congress*, Taipei, Taiwan, October 25–30, 2015; 562–569.
88. Raisee M, Kumar D, Lacor C. A non-intrusive model reduction approach for polynomial chaos expansion using Proper Orthogonal Decomposition. *International Journal for Numerical Methods in Engineering* 2015; **103**(4):293–312.
89. Peherstorfer B, Willcox K. Data-driven operator inference for nonintrusive projection-based model reduction. *Computer Methods in Applied Mechanics and Engineering* 2016; **306**:196–215.
90. Lin Z, Xiao D, Fang F, Pain C, Navon IM. Non-intrusive reduced order modelling with least squares fitting on a sparse grid. *International Journal for Numerical Methods in Fluids* 2017; **83**:291–306, 10.1002/fld.4268.

DOI: 10.1002/nme